Boundary-Layer Meteorol (2018) 166:137–151
https://doi.org/10.1007/s10546-017-0295-5

RESEARCH ARTICLE

Initializing a Mesoscale Boundary-Layer Model with Radiosonde Observations

Guillermo J. Berri[1,2] · Germán Bertossa[3,4]

Received: 23 December 2016 / Accepted: 10 August 2017 / Published online: 19 August 2017

Abstract A mesoscale boundary-layer model is used to simulate low-level regional wind fields over the La Plata River of South America, a region characterized by a strong daily cycle of land–river surface-temperature contrast and low-level circulations of sea–land breeze type. The initial and boundary conditions are defined from a limited number of local observations and the upper boundary condition is taken from the only radiosonde observations available in the region. The study considers 14 different upper boundary conditions defined from the radiosonde data at standard levels, significant levels, level of the inversion base and interpolated levels at fixed heights, all of them within the first 1500 m. The period of analysis is 1994–2008 during which eight daily observations from 13 weather stations of the region are used to validate the 24-h surface-wind forecast. The model errors are defined as the root-mean-square of relative error in wind-direction frequency distribution and mean wind speed per wind sector. Wind-direction errors are greater than wind-speed errors and show significant dispersion among the different upper boundary conditions, not present in wind speed, revealing a sensitivity to the initialization method. The wind-direction errors show a well-defined daily cycle, not evident in wind speed, with the minimum at noon and the maximum at dusk, but no systematic deterioration with time. The errors grow with the height of the upper boundary condition level, in particular wind direction, and double the errors obtained when the upper boundary condition is defined from the lower levels. The conclusion is that defining the model upper boundary condition from radiosonde data closer to the ground minimizes the low-level wind-field errors throughout the region.

✉ Guillermo J. Berri
gberri@smn.gov.ar

1 Servicio Meteorológico Nacional - Conicet, Avda. Dorrego 4019, C1425GBE Ciudad de Buenos Aires, Argentina

2 Present Address: Facultad de Ciencias Astronómicas y Geofísicas - Conicet, Universidad Nacional de La Plata, Paseo del Bosque s/n, B1900FWA La Plata, Argentina

3 Servicio Meteorológico Nacional, Buenos Aires, Argentina

4 Present Address: Silvercloud, Buenos Aires, Argentina

Keywords Boundary-layer model · Forecast errors · Initialization data · Low-level wind fields · Radiosonde observations

1 Introduction

The La Plata River in South America is a large water surface 300 km long, with a variable width between 40 and 200 km (see Fig. 1). This region creates a considerable surface-temperature contrast with the continent that sets up the appropriate conditions for the development of a low-level circulation of sea–land breeze type. This circulation is generated by the daily cycle of the surface-temperature contrast between land and river, so that flow tends to be from water to land during the day and from land to water at night. Figure 2 presents the mean wind direction observed at 13 weather stations in the region during the period 1994–2008. Figure 2a, which corresponds to 0600 LST (local standard time) just before sunrise during most of the year, shows predominant offshore winds, particularly over the northern coast. At 1500 LST (mid-afternoon), Fig. 2b shows dominant onshore winds almost everywhere in the region. This notable change observed in the predominant flow between the times of maximum and minimum temperatures clearly indicates the significant role played by the sea–land breeze circulation in the local climatology.

Berri et al. (2010) presented an ensemble method for simulating the high-horizontal- resolution low-level climatological wind fields, i.e., the result of long-term weather conditions, over the La Plata River region using a mesoscale boundary-layer model. In that study‘ the boundary-layer model is forced by local weather observations and the climatological wind field is calculated with a reduced number of daily forecasts, each characterized by given wind-direction and wind-speed classes defined at the model top. Each forecast, or ensemble member, participates in the calculation of the mean wind field multiplied by the relative frequency with which the given wind condition occurs in the database.

The upper boundary condition was taken from the 0900 LST observation of the only radiosonde station available in the region, and the lower boundary condition was a surface-heating function calculated with the surface-temperature observations of the region. Berri et al. (2010), in a study covering the 25-year period 1959–1984, revealed an overall good

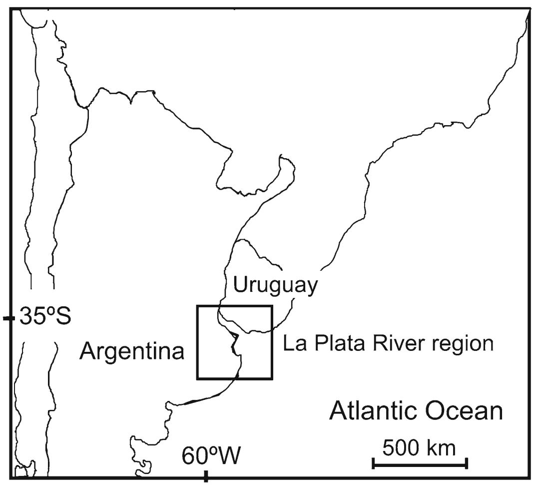

Fig. 1 Location of La Plata River region in South America

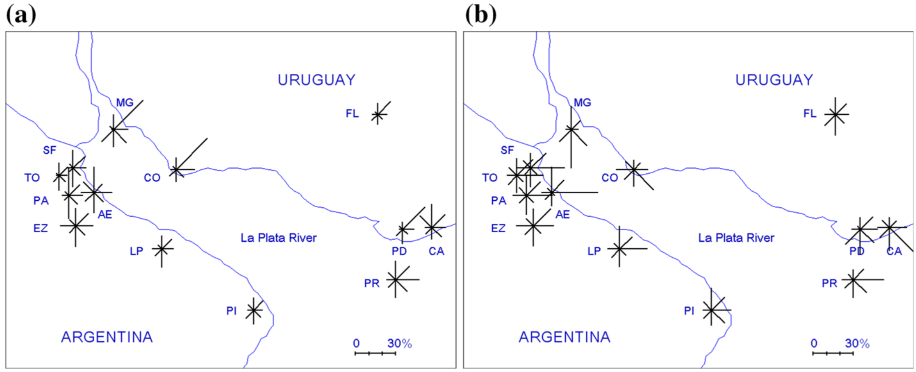

Fig. 2 Observed 1994–2008 mean wind direction frequencies at, **a** 0600 local time, and **b** 1500 local time. The *bars* indicate the wind direction with a relative frequency according to the percentage scale shown in the *lower right corner* of each figure. The surface weather stations of the study are: Florida (FL), Carrasco (CA), Prado (PD), Colonia (CO), Martín García (MG), San Fernando (SF), Don Torcuato (TO), El Palomar (PA), Ezeiza (EZ), Aeroparque (AE), La Plata Aero (LP), Punta Indio (PI), and Pontón Recalada (PR)

agreement between observed and modelled winds, and concluded that the ensemble method with the BLM model was useful for synthesizing high-resolution climatological low-level wind fields over regions with a strong diurnal cycle of surface thermal contrast. For the definition of the 25-year climatological wind field, Berri et al. (2010) used the 1000-hPa level to define the upper boundary condition of the boundary-layer model, with a vertical domain (2-km depth) confined within the atmospheric boundary layer. The decision to use the 1000-hPa level was based on Sraibman and Berri (2009), who compared the results of the boundary-layer model validation using the first three standard radiosonde levels, i.e., 1000, 925 and 850 hPa, with the 1000-hPa level giving the best result. The authors concluded that the result was due to the fact that the other two standard levels were located, in most cases, above the temperature inversion base, despite the fact that the mean height of 160 m for the 1000-hPa level was too low to be considered as the boundary-layer top. Both studies used four daily observations (0300, 0900, 1500 and 2100 LST) from five weather stations. Recently, a more complete database of the region was created that includes eight 3-h observations (0000, 0300 and so on until 2100 LST), from 13 weather stations of the region. In addition to that, the radiosonde database available now is more complete, including not only the standard (fixed) levels but also the significant levels (variable in number and height), which provide more details on the vertical structure of the boundary layer. Significant levels are those in which the changes in temperature and/or moisture content are significant for determining weather conditions, and allow a reasonably accurate reproduction of the radiosonde observation by simple interpolation between levels.

The availability of the new 1994–2008 database motivated the interest in reviewing previous studies with the purpose of optimizing the use of the boundary-layer model to synthesize low-level climatological wind fields over regions with limited observations available and characterized by a strong diurnal cycle in surface thermal contrast. Therefore, the objective of the present study is to evaluate different criteria for choosing the radiosonde observation level that will serve to initialize the top boundary condition of the boundary-layer model. Section 2 briefly describes the boundary-layer model formulation and the experimental design, Sect. 3 describes how boundary conditions are defined, and Sect. 4 presents the methodology for the calculation of the climatological wind fields and the validation method. Section 5 discusses results and the conclusions, and a final discussion is presented in Sect. 6.

2 BLM Model and Experiment Design

The boundary-layer model is based on a dry, hydrostatic boundary layer and includes the basic conservation equations of momentum, mass and heat, with a first-order turbulence closure; see Berri et al. (2010) for details of the model formulation. In brief, the boundary-layer model has been specifically developed for simulating the low-level circulation over coastal regions, and is driven by prescribed upper and lower boundary conditions defined from the observations. The model domain for the experiments, as well as the location of the 13 weather stations used in the study, can be seen in Fig. 2. The horizontal resolution is 0.05∘, which corresponds to an average of 5 km, with 79 points in the x direction (354 km) and 58 points in the y direction (316 km). The vertical domain has 12 levels between the surface and the material top at 2000 m, distributed according to a log-linear spacing.

As mentioned above, the ensemble method of Berri et al. (2010) considers a set of 192 members (16 wind-direction sectors of 22.5° and 12 wind-speed classes at the boundary-layer top). The wind-speed classes are defined by the following upper limits: 2, 3, 4, 5, 6, 7, 8, 9, 10, 12, 14 and $>14\,\mathrm{m\,s^{-1}}$. The mean wind field is calculated by averaging the 192 members, each one multiplied by the relative frequency with which the given wind condition occurs in the database. Berri et al. (2012) verified the ability of the ensemble method in synthesizing low-level wind fields over the La Plata River region, by comparing results with the conventional method that simply averages the whole set of individual daily forecasts. The later study considered 3248 realizations during the period 1959–1984, employing four daily observations from five weather stations for the validation of results. Both methods used the same set of observations, study period, and upper and lower boundary conditions, so that the differences are only due to the post-processing of the forecast results. Berri et al. (2012) concluded that there was no clear advantage of one method over the other, since the errors in both cases were similar. Considering this result, we decided to use all possible daily forecasts during the period 1994–2008 for validating the climatological wind fields obtained with the boundary-layer model. The particular advantage is that the modelled wind fields are validated, at every weather station, only with those days and times with available observations since not all of them coincide with their periods of data availability.

3 Boundary Conditions

The upper boundary condition for temperature and wind is taken from the 0900 LST Ezeiza station radiosonde observation (EZ in Fig. 2). Since there is only one radiosonde observation daily, the upper boundary condition remains constant during the 24-h forecast. The lower boundary condition for surface temperature is defined as a function of time by means of a cubic spline interpolation of nine consecutive 3-h observations from 0600 LST of the day of forecast until 0600 LST of the following day. The model run starts at 0600 LST and the first validation time is 0900 LST, so that the first 3 h are allowed for the model spin-up. Two weather stations are chosen for determining the surface temperature, one inland, Ezeiza station (EZ in Fig. 2), and the other one in the river, Pontón Recalada station (PR in Fig. 2). Ezeiza station is chosen because it is the radiosonde station used in our study, and Pontón Recalada station because it is the only river station located on a ship anchored away from the coast, so that it provides a good representation of the meteorological conditions in the river. At every grid point over land (river), the surface temperature is obtained from the interpolation of the observations at Ezeiza station (Pontón Recalada station). At the lateral boundaries, all variables are allowed to change in order to provide a zero gradient across the boundaries at each timestep, except for the pressure since its gradient provides the geostrophic wind speed. Only those days with complete observations at Ezeiza station (surface and radiosonde) and Pontón Recalada station (surface) are included herein.

A key aspect is the selection of the radiosonde level that defines the top boundary condition of the model that, conceptually, should be the boundary-layer height (H). However, there is no a universal definition since H is variable and depends on the meteorological conditions at the time of the observation and the physical characteristics of the site. Pielke (2002) provides a rich discussion (p. 188, and references therein) of the different criteria used to determine H. For example Blackadar and Tennekes (1968) determine H in terms of the ratio between surface friction velocity and the Coriolis parameter; Oke (1978) defines H in terms of the temperature inversion; and Krishnamurti et al. (1983) determine H from the balance of pressure, Coriolis and frictional forces. Seibert et al. (2000) review different methods for determining the height of the mixing layer and make recommendations on the analysis of profile measurements and the use of parametrization schemes and simple models. In particular Ulke and Mazzeo (1998) analyzed the mixing height over the city of Buenos Aires and its variability for different seasons of the year. In general, these studies discuss different methods for determining the height of the mixing layer and they mainly focus on the afternoon hours; some studies require additional information not available in the standard weather observations of the region. However, the only daily radiosonde observation available in the region is in the early morning, when the boundary layer is shallow, so that we have no means of determining the daily evolution of wind speed and temperature at $z = H$ as required for defining the upper boundary condition. Therefore, we consider the following four groups of cases for defining the upper boundary condition from the 0900 LST radiosonde observation, which remains constant during the whole integration period:

(i) standard levels (STD) at 1000 hPa (STD_{1000}), 925 hPa (STD_{925}) and 850 hPa (STD_{850}).
(ii) first significant level (SIG) between 50 and 200 m (SIG_{50-200}) and between 200 and 400 m ($SIG_{200-400}$). According to the meteorological standards, significant levels are those points ascertained from the plotted sounding where a significant change in the temperature and/or dewpoint profile is detected.
(iii) level of the temperature inversion base (IVB) between 50 and 300 m (IVB_{50-300}), between 300 and 600 m ($IVB_{300-600}$), between 600 and 1000 m ($IVB_{600-1000}$), and between 1000 and 1500 m ($IVB_{1000-1500}$).
(iv) interpolated level at fixed heights (INT) of 300 m (INT_{300}), 600 m (INT_{600}), 900 m (INT_{900}), 1200 m (INT_{1200}) and 1500 m (INT_{1500}).

All cases with a resulting height below 50 m are excluded because they were not considered representative of the boundary-layer conditions due to the proximity to the ground. Table 1 summarizes the 14 upper boundary conditions used with an indication of the number of days that participate for each case. It must be pointed out that the 0900 LST radiosonde sounding is in the morning when the boundary layer is not fully developed, which may affect the results.

Table 1 Levels employed for defining the model upper boundary condition, with the corresponding number of days

Standard level number of cases	STD_{1000} 3196	STD_{925} 3218	STD_{850} 3201		
First significant level number of cases	SIG_{50-200} 1000	$SIG_{200-400}$ 1120			
Temperature inversion base level number of cases	IVB_{50-300} 656	$IVB_{300-600}$ 633	$IVB_{600-1000}$ 528	$IVB_{1000-1500}$ 388	
Interpolated level at fixed height number of cases	INT_{300} 2847	INT_{600} 2866	INT_{900} 2874	INT_{1200} 2867	INT_{1500} 2866

4 Validation of the Climatological Wind Field

The validation of the climatological wind field is performed by comparing the observed wind vector at 13 surface weather stations in the region (see Fig. 2) with the wind forecast obtained with the boundary-layer model. The four grid points that surround each weather station are considered, provided they share the same surface characteristics of either land or water, and that the minimum error is adopted. The wind observations correspond to nine surface weather stations in Argentina (Ezeiza, Aeroparque, Don Torcuato, La Plata, Martin Garcia, Palomar, Punta Indio, San Fernando and Pontón Recalada) and four stations in Uruguay (Carrasco, Colonia, El Prado and Florida). The data correspond to years 1994–2008 and the model results are validated at 3-h intervals from 0900 LST until 0060 LST of the following day.

The World Meteorological Organization Manual on Codes (WMO 2015) establishes that observations of wind direction must be recorded in tens of degrees, for example 18 for southerly direction, 36 for northerly direction, etc. Figure 3a shows the number of wind-direction observations per decade (tens of degrees from 01 to 36) recorded at Ezeiza station during the period 1994–2008. It can be clearly seen that the data are biased because some decades contain barely one or two observations, for example 01, and in some cases there are two consecutive decades, for example 03 and 04. The observations are concentrated in the 16 main sectors of the wind rose, i.e., north, north-north-east, north-east, and so on, (see Fig. 3b) that correspond to the decades (in degrees) 36, 02, 05, and so on, respectively. However, a closer inspection of the data reveals another problem that can be appreciated in Fig. 3b, which shows that the distribution of wind direction in the 16 main sectors has a sawtooth shape. There is a set of eight wind directions (north, north-east, east, south-east, south, south-west, west and north-west) with consistently higher frequencies than another set of intermediate eight wind directions (north-north-east, east-north-east, east-south-east, south-south-east, south-south-west, west-south-west, west-north-west and north-north-west). The first set corresponds to the eight main sectors of the wind rose and the second set corresponds to the eight intermediate ones. All other weather stations used in the study have the same problem.

The observations are automatically recorded and archived by the National Meteorological Service as soon as the SYNOP messages are received. These messages are manually encoded by the observer on duty at the weather station and sent every hour to headquarters by all weather stations in the network. There is no physical reason that can explain such a distribution

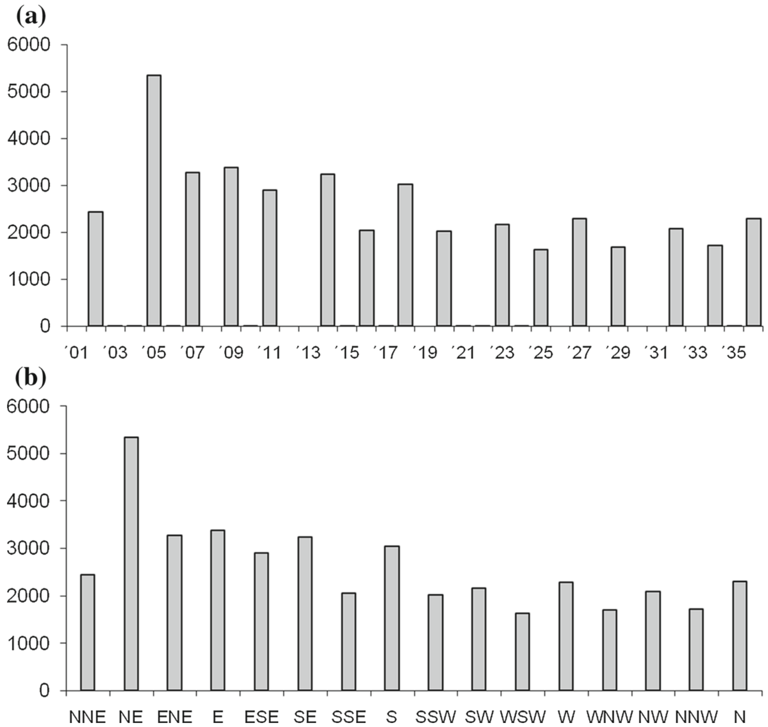

Fig. 3 Number of observations at Ezeiza station during 1994–2008 as a function of the wind direction expressed, **a** in tens of degrees from the north, **b** in the conventional 16-sector wind rose

of wind directions so that it has to be considered a systematic error in the observational system. In view of this problem it was decided to rearrange the data by redistributing the isolated observations and the observations in the eight intermediate wind directions into the eight main wind directions, proportionally to the number of cases in the two contiguous main wind directions. Consequently, the width of the wind direction sectors adopted for the validation is 45°.

Each forecast gives the horizontal wind components u and v at a height of 10 m, which can be expressed as a wind direction D (degrees from the north), and a wind speed (m s^{-1}) $V = (u^2 + v^2)^{1/2}$. The wind direction D defines the wind sector identified as one in the 8-sector wind rose. Calm conditions are defined as those cases when the wind speed is smaller than a given threshold, since the model is unable to predict a zero wind speed. The calm threshold is adjusted for each observing time and weather station by running model simulations with variable thresholds until the resulting percentage of calm conditions matches the observed one. Once the set of model runs is completed, the modelled wind-direction frequency distribution f_i (percentage), and mean wind speed per wind sector V_i (m s^{-1}) are calculated (i = 1–9, corresponding to eight wind sectors plus calm). Then, f_i and V_i are compared to the observed wind-direction frequency distribution and mean wind speed per wind sector fo_i and Vo_i, respectively, and the errors calculated. The model errors are defined as the root-mean-square of the relative error (*RMSE*) in wind-direction frequency $E(D)$, and in mean wind speed per wind sector $E(V)$, both weighted by the mean observed wind-direction frequency fo_i, as follows,

$$E(D) = \left[\sum_{i=1}^{9} fo_i (eD_i)^2 \Big/ \sum_{i=1}^{9} fo_i \right]^{1/2}, \quad (1)$$

$$E(V) = \left[\sum_{i=1}^{9} fo_i (eV_i)^2 \Big/ \sum_{i=1}^{9} fo_i \right]^{1/2}, \quad (2)$$

where $eD_i = (f_i - fo_i)/fo_i$ and $eV_i = (V_i - Vo_i)/Vo_i$ are the relative errors in wind direction and wind speed, respectively. For simplicity, the *RMSE* values for (1) and (2) will be simply referred to as wind-direction (W_{dir}) and wind-speed (W_{spd}) errors, respectively.

5 Results

The analysis of model errors is done separately for wind direction and wind speed since the wind-direction observations show significant changes of predominant wind sectors across the region with the time of day, while wind speed is less variable. Figure 4 presents the W_{dir} errors, and Fig. 5 the W_{spd} errors, of the 14 upper boundary conditions, as the mean value of the whole period of every weather station. The first nine stations plotted in Figs. 4 and 5 are in Argentina and the last four in Uruguay, with no particular order for each group.

In general, W_{dir} errors are larger than W_{spd} errors and show greater dispersion among the different upper boundary conditions, between 30 and 70% in W_{dir} in comparison to less than 25% in W_{spd}, indicating that W_{dir} is clearly more sensitive than $W_{spd}$to the initialization

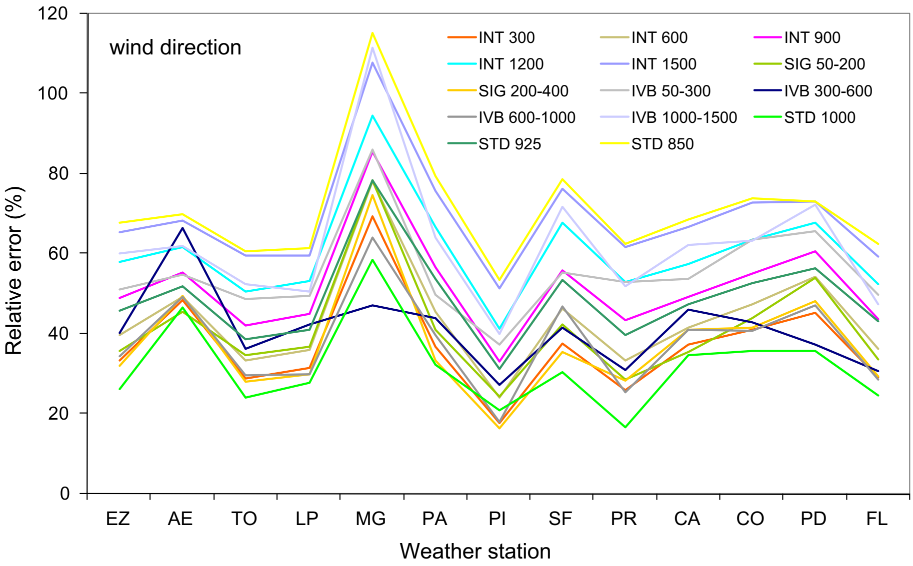

Fig. 4 Percentage *RMSE* values (relative errors) in wind direction (see Eq. 1) for the 14 upper boundary conditions (see Table 1 for the details). The meteorological stations are: Florida (FL), Carrasco (CA), Prado (PD), Colonia (CO), Martín García (MG), San Fernando (SF), Don Torcuato (TO), El Palomar (PA), Ezeiza (EZ), Aeroparque (AE), La Plata Aero (LP), Punta Indio (PI), and Pontón Recalada (PR). The period of analysis is 1994–2008

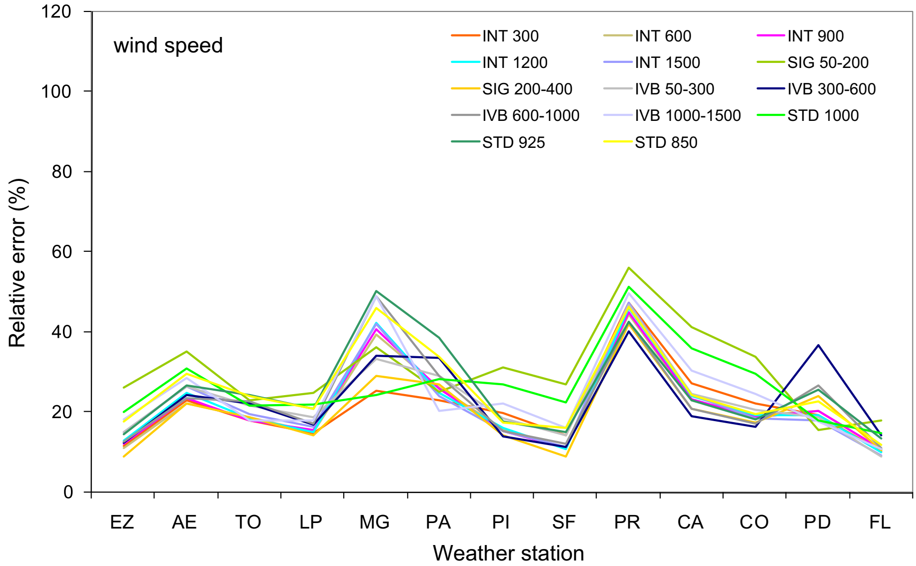

Fig. 5 Same as Fig. 4 but for wind speed (see Eq. 2)

method. STD_{1000} is the upper boundary condition with the minimum W_{dir} error in all but three weather stations, while in the case of W_{spd} there is no clear predominance of a particular upper boundary condition with maximum or minimum errors. MG station has the largest W_{dir} errors in most upper boundary conditions, while PR station shows the largest W_{spd} errors, followed by MG station. The other weather stations show errors of similar magnitudes. The particular characteristics of the MG station site could be the reason for the largest error since it is located on a small island about 3 km wide, a dimension that the model resolution of 5 km cannot appropriately handle. The PR station is on a ship in the river, and the anemometer is mounted on a tower at 21 m above the sea level. Although this situation was taken into consideration for the validation process, since the model results for this location relate to a height of 21 m rather than of the standard height of 10 m for all the other locations, the particular characteristics of this site may explain the large W_{spd} error.

With respect to the time of the day, Fig. 6 shows the W_{dir} errors and Fig. 7 the W_{spd} errors, as the average of all weather stations. The time axis runs from 0900 LST, the initial validation time, to 0600 LST of the following day, the end of each daily forecast. W_{dir} errors are again larger than W_{spd} errors and show greater dispersion among the different upper boundary conditions. W_{dir} errors show a daily cycle, not so evident in W_{spd}, with the minimum at noon and the maximum at 2100 LST, evident in all cases with the exception of $IVB_{300-600}$ whose maximum is at 1500 LST and minimum at 0300 LST. Interestingly, the W_{dir} forecast does not show a systematic deterioration with time as might be expected. Initially there is a reduction in the W_{dir} error, indicating that the model capacity in reproducing the dominant influence of the daily cycle of land-river temperature contrast. As the land–river temperature difference increases, the typical inland component of the sea-breeze circulation is affected, making the forecast less dependent on the initial conditions. By mid-afternoon the W_{dir} errors grow, reach their largest values at 2100 LST, and from then on decrease towards values similar to the beginning of the forecast. This behaviour suggests an inability of the model to simulate the transition from unstable to stable conditions in the late evening. The stability

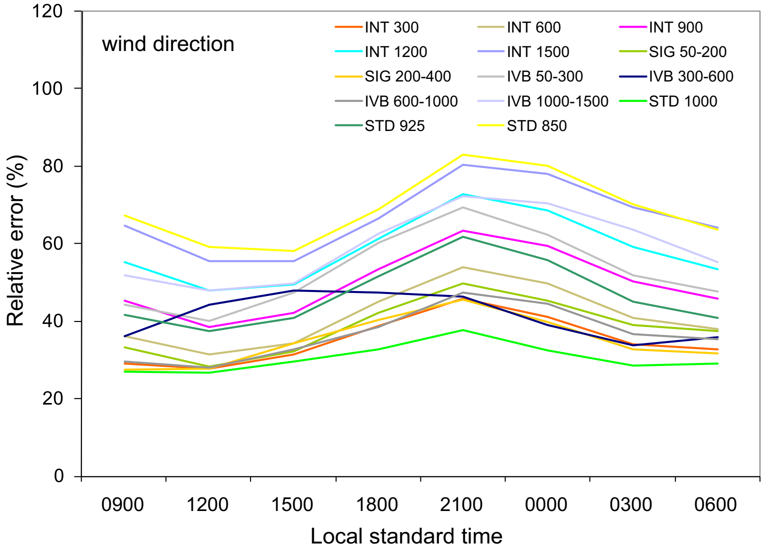

Fig. 6 Percentage *RMSE* values (relative errors) in wind direction (see Eq. 1), averaged of the 13 weather stations of the study as a function of the local standard time

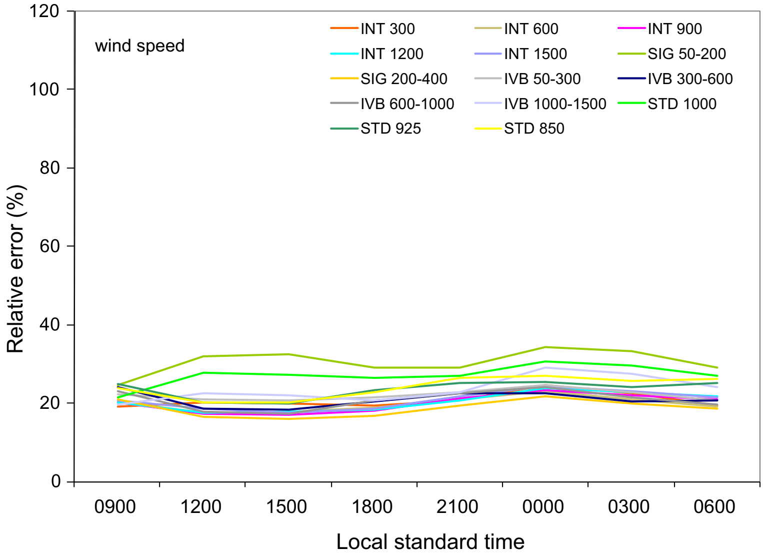

Fig. 7 Same as Fig. 6 but for wind speed (see Eq. 2)

conditions are determined as a function of the vertical temperature gradient in the surface layer, based on the principles of the Monin–Obukhov similarity theory. For details on the model calculations and the parametrization schemes used, see Berri and Nuñez (1993). Thus, the change with time of the vertical stability is driven by the change with time of the surface temperature, which results from the interpolation of temperature observations every 3 h.

Table 2 W_{dir} errors of the 14 upper boundary conditions at the 13 weather stations, averaged of the eight daily validation times

	EZ	AE	TO	LP	MG	PA	PI	SF	PR	CA	CO	PD	FL
INT_{300}	33	48	29	32	69	37	18	38	26	37	*41*	45	*29*
INT_{600}	40	49	33	36	78	45	24	46	34	42	47	54	36
INT_{900}	49	55	42	45	85	57	33	56	44	49	55	61	44
INT_{1200}	58	62	51	53	95	67	41	68	53	57	64	68	52
INT_{1500}	65	68	60	60	108	76	51	76	62	67	73	73	59
SIG_{50-200}	36	**46**	35	37	78	41	24	42	29	*36*	44	54	34
$SIG_{200-400}$	*32*	50	*28*	30	75	*33*	**17**	*35*	28	41	42	48	*29*
IVB_{50-300}	51	55	49	50	86	50	37	55	53	54	64	66	50
$IVB_{300-600}$	40	66	36	42	**47**	44	27	42	31	46	43	*37*	31
$IVB_{600-1000}$	34	49	30	*30*	64	40	*18*	47	*25*	41	*41*	47	*29*
$IVB_{1000-1500}$	60	62	52	51	112	64	40	72	52	62	63	72	47
STD_{1000}	**26**	*47*	**24**	**28**	*59*	**32**	21	**30**	**17**	**35**	**36**	**36**	**25**
STD_{925}	46	52	39	41	78	54	31	53	40	47	53	56	43
STD_{850}	68	70	61	62	115	79	53	79	63	69	74	73	63

Bold values highlight the absolute minimum error and italic values the following relative minimum

Since the transition between stability conditions in the evening occurs earlier in winter and later in summer, the 3-h data resolution may be insufficient.

The minimum W_{dir} error at all times is obtained with STD_{1000} (Fig. 6), while STD_{850} gives the largest W_{dir} error at all times. In the case of W_{spd} (Fig. 7), the errors show independence of time as well as no deterioration with time. $SIG_{200-400}$ provides the minimum W_{spd} error at all times, almost without exception, while SIG_{50-200} always has the largest W_{spd} error.

Table 2 presents the W_{dir} errors of the different upper boundary conditions as the average of the eight daily validation times for each weather station. The absolute minimum value and the following relative minimum value are highlighted in bold and italic values, respectively. STD_{1000} is the upper boundary condition with a minimum W_{dir} error in 10 out of 13 weather stations, while two of them have the following relative minimum, and in only one weather station is left in third place although by a few percentage points. Considering the wind-direction errors, $STD_{1000}$is the overall best upper boundary condition option since it gives the minimum error in the majority of places across the region.

In the case of W_{spd} (see Table 3), the best performance is obtained with $SIG_{200-400}$ (six out of 13 weather stations), followed by $IVB_{300-600}$ (four out of 13 weather stations). However, there is no clear advantage of a particular upper boundary condition over the others since there are several weather stations in which two or more upper boundary conditions share the absolute minimum error, and the difference between the absolute minimum error and the other relative minima is quite small.

When considering the arithmetic average of W_{dir} and W_{spd} errors, defined as the W_{ave} error (see Table 4), the clear advantage obtained with STD_{1000} for W_{dir} fades away. It is $SIG_{200-400}$that now gives the best result in 10 out of 13 weather stations, followed by STD_{1000} in six, and other upper boundary conditions in five and four weather stations.

Figure 8 shows the W_{dir} and W_{spd} errors, averaged of all validation times and weather stations, as a function of the mean height of the 14 upper boundary conditions studied (see Table 5). W_{dir} shows a clear dependence with height since the errors double from about 30%

Table 3 W_{spd} errors of the 14 upper boundary conditions at the 13 weather stations, averaged of the eight daily validation times

	EZ	AE	TO	LP	MG	PA	PI	SF	PR	CA	CO	PD	FL
INT_{300}	12	*23*	**18**	*15*	*26*	*23*	20	14	47	27	22	19	*10*
INT_{600}	*11*	**22**	19	*15*	40	26	16	*11*	44	23	19	20	11
INT_{900}	12	24	**18**	16	41	26	*15*	*11*	45	23	19	20	11
INT_{1200}	13	25	*19*	*15*	42	25	16	*11*	46	24	19	19	*10*
INT_{1500}	15	26	20	16	42	24	*15*	*11*	47	24	19	*18*	*9*
SIG_{50-200}	26	35	23	25	36	25	31	27	56	41	34	**16**	18
$SIG_{200-400}$	**9**	**22**	*19*	**14**	29	27	**14**	**9**	*42*	*21*	**17**	24	11
IVB_{50-300}	15	27	22	19	33	29	19	14	47	25	21	19	**9**
$IVB_{300-600}$	13	24	22	17	34	34	**14**	*11*	**40**	**19**	**17**	37	14
$IVB_{600-1000}$	13	24	23	17	49	29	*15*	12	43	*21*	**17**	27	11
$IVB_{1000-1500}$	18	29	**18**	18	49	**20**	22	16	50	31	25	*18*	11
STD_{1000}	20	31	22	22	**24**	28	27	23	51	36	30	*18*	15
STD_{925}	15	27	24	21	50	39	18	15	43	23	*18*	*26*	13
STD_{850}	18	30	24	21	46	34	17	16	46	24	20	23	12

Bold values highlight the absolute minimum error and italic values the following relative minimum

Table 4 W_{ave} errors (defined as the arithmetic average of W_{dir} and W_{spd}) of the 14 upper boundary conditions at the 13 weather stations, averaged of the eight daily validation times

	EZ	AE	TO	LP	MG	PA	PI	SF	PR	CA	CO	PD	FL
INT_{300}	*23*	**36**	**23**	*23*	*47*	**30**	19	*26*	37	*32*	32	*32*	**20**
INT_{600}	25	**36**	*26*	26	59	36	20	29	39	*32*	33	37	24
INT_{900}	31	*39*	30	30	63	41	24	34	44	36	37	41	27
INT_{1200}	36	43	35	34	68	46	29	39	50	41	41	44	31
INT_{1500}	40	47	40	38	75	50	33	44	55	45	46	45	34
SIG_{50-200}	31	40	29	31	57	*33*	28	35	42	38	39	35	26
$SIG_{200-400}$	**21**	**36**	**23**	**22**	52	**30**	**15**	**22**	*35*	**31**	**29**	36	**20**
IVB_{50-300}	33	41	35	34	60	39	28	35	50	39	42	42	29
$IVB_{300-600}$	26	45	29	30	**41**	39	21	27	36	33	*30*	37	*23*
$IVB_{600-1000}$	24	**36**	*26*	24	57	34	*17*	30	**34**	**31**	**29**	37	**20**
$IVB_{1000-1500}$	39	45	35	34	80	42	31	44	51	46	44	45	29
STD_{1000}	*23*	*39*	**23**	25	**41**	**30**	24	*26*	**34**	35	33	**27**	**20**
STD_{925}	30	*39*	31	31	64	46	25	34	41	35	35	41	28
STD_{850}	43	50	42	41	81	57	35	47	54	46	47	48	37

Bold values highlight the absolute minimum error and italic values the following relative minimum

for the upper boundary condition cases with mean heights closer to the ground, to about 60% of those at upper levels. In the case of wind speed the errors are independent of the upper boundary condition height.

Other studies calculate surface wind-vector errors using individual forecasts instead of mean frequency distributions of wind direction and wind speed, as in our study. For example,

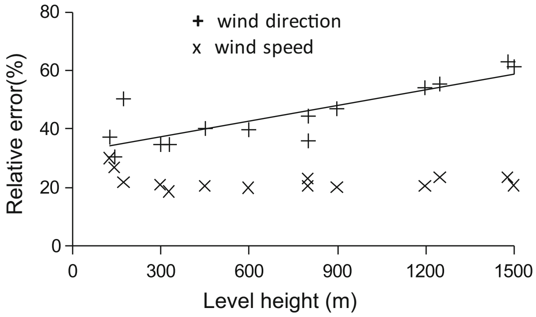

Fig. 8 Mean value of W_{dir} (+) and W_{spd} (×) relative errors in the surface wind as a function of the mean height of the 14 upper boundary conditions studied (see Table 2)

Table 5 W_{dir} and W_{spd} errors, averaged of the eight daily validation times and the 13 weather stations, as a function of the upper boundary condition mean height

	Level height	W_{dir} error	W_{spd} error
INT_{300}	300	35	21
INT_{600}	600	40	20
INT_{900}	900	47	20
INT_{1200}	1200	54	20
INT_{1500}	1500	61	21
SIG_{50-200}	125	37	30
$SIG_{200-400}$	330	35	19
IVB_{50-300}	175	50	22
$IVB_{300-600}$	450	40	21
$IVB_{600-1000}$	800	36	21
$IVB_{1000-1500}$	1250	55	24
STD_{1000}	142	30	27
STD_{925}	801	45	23
STD_{850}	1480	63	24

Case et al. (2002) find that the 24-h RAMS model forecast over Florida has *RMSE* values in wind direction of 30°–60° and *RMSE* values in wind speed of 1–3 m s^{-1}; and Wyszogrodzki et al. (2013) find an *RMSE* of 85°–100° and of 1–2 m s^{-1} for wind direction and wind speed, respectively, with 24-h WRF model forecasts over the contiguous USA. All but one of the weather stations used herein have mean wind speeds <5 m s^{-1}, so that the relative *RMSE* of 20–30% for wind speed would be equivalent, at most, to 1.5 m s^{-1}, similar to other studies. In the case of wind direction the comparison is more difficult since the present study considers categorical agreement within 45-deg sectors instead of the angular difference between forecast and observation, used elsewhere. For example, Wyszogrodzki et al. (2013) give *RMSE* values of 85°–100° that would be equivalent to a forecast outside the 45-deg wind-direction sector in the majority of cases, which in turn would represent a greater *RMSE* (relative error) than the average 40% found here. Using the same argument, the *RMSE* value in Case et al. (2002) of 30°–60° would probably represent a similar but not much smaller *RMSE* (relative error) than ours. Despite both methods being not strictly compatible, it can be stated that the errors in wind direction and wind speed are equivalent to those in other studies.

6 Discussion and Conclusions

We have evaluated different criteria for choosing the radiosonde observation level used to initialize the upper boundary condition of a boundary-layer model. The ultimate purpose was to optimize the use of the model to synthesize low-level climatological wind fields over regions with limited observations available, and characterized by a strong diurnal cycle in land–river surface thermal contrast. A more complete database of radiosonde and surface meteorological observations than that available in previous studies was used to validate the 24-h low-level wind forecast. The study considers 14 upper boundary conditions defined from the radiosonde data at standard levels, significant levels, level of the inversion base and interpolated levels at fixed heights, all within the first 1500 m above the ground. The model errors are defined as the root-mean-square of the relative error of W_{dir} and W_{spd}.

The results show that W_{dir} errors are greater than W_{spd} errors, and display a significant dispersion among the different upper boundary conditions, not present in W_{spd}, revealing a sensitivity to the initialization method. W_{dir} errors also show a well-defined daily cycle, not evident in W_{spd}, with the minimum at 1200 LST and the maximum at 2100 LST, present in all but one of the upper boundary conditions studied. This is a consequence of the significant change throughout the day of the wind direction with highest frequency (wind speed is less variable), due to the sea–land breeze type of circulation that is dominant in the region. Interestingly, the W_{dir} forecast does not show a systematic deterioration with time as is usual in weather prediction. The errors show a clear dependence on the height of the radiosonde level used for defining the model upper boundary condition, in particular W_{dir}, since the errors grow with height and double those obtained with the upper boundary condition defined from the lower levels. Clearly, defining the model upper boundary condition from radiosonde levels closer to the ground minimizes the low-level wind-field errors throughout the region.

In terms of the practical use of this methodology, STD_{1000} is the most convenient choice since it is always available from radiosonde observations and does not require any additional calculations. In this sense, this confirms the results of previous studies (Berri et al. 2010, 2012), who found the first standard level of 1000 hPa as the most appropriate one. The availability of a single daily radiosonde observation is a limiting factor because this forces the upper boundary condition to be constant during the whole forecast period. More daily radiosonde observations would allow a better representation of the changes in the meteorological conditions during the forecast period, which should contribute to forecast improvement. Another limiting factor is that the radiosonde observation is at 0900 LST when the boundary layer is shallow. In this sense, having the single radiosonde observation in the afternoon would be more desirable since it would provide information of a completely developed mixing layer.

Acknowledgements This research was partially supported by research grant PICT2012–1667 from Agencia Nacional de Promoción Científica y Tecnológica of Argentina. Also acknowledged is Servicio Meteorológico Nacional of Argentina for providing the meteorological data, with special thanks to the Department of Data Processing.

References

Berri GJ, Nuñez MN (1993) Transformed shoreline following horizontal coordinates in a mesoscale model: a sea land breeze case study. J Appl Meteorol 32:918–928

Berri GJ, Sraibman L, Tanco RA, Bertossa G (2010) Low-level wind field climatology over the La Plata River region obtained with a mesoscale atmospheric boundary layer model forced with local weather observations. J Appl Meteorol 49:1293–1305

Berri GJ, Galli Nuin J, Sraibman L, Bertossa G (2012) Verification of a synthesized method for the calculation of low-level climatological wind fields using a mesoscale boundary-layer model. Boundary-Layer Meteorol 142:329–337

Blackadar AK, Tennekes H (1968) Asymptotic similarity in neutral barotropic planetary boundary layers. J Atmos Sci 25:1015–1020

Case JL, Manobianco J, Dianic AV, Wheeler MM, Harms DE, Parks CR (2002) Verification of high-resolution RAMS forecasts over East-Central Florida during the 1999 and 2000 summer months. Weather Forecast 17:1133–1151

Krishnamurti TN, Wong V, Pan H-L, Pasch R, Molinari J, Ardanu P (1983) A three-dimensional planetary boundary layer model for the Somali jet. J Atmos Sci 40:894–908

Oke TR (1978) Boundary layer climates. Methuen, London

Pielke RA (2002) Mesoscale meteorological modeling. Academic Press, New York

Seibert P, Beyrich F, Gryning SE, Joffre S, Rasmussen A, Tercier P (2000) Review and intercomparison of operational methods for the determination of the mixing height. Atmos Environ 34:1001–1027

Sraibman L, Berri GJ (2009) Low level wind forecast over La Plata River region with a mesoscale boundary layer model forced by regional operational forecasts. Boundary-Layer Meteorol 130:407–422

Ulke A, Mazzeo NA (1998) Climatological aspects of the daytime mixing height in Buenos Aires City, Argentina. Atmos Environ 32:1615–1622

World Meteorological Organization (2015) Manual on codes. WMO No. 306

Wyszogrodzki AA, Liu Y, Jacobs N, Childs P, Zhang Y, Roux G, Warner T (2013) Analysis of the surface temperature and wind forecast errors of the NCAR-AirDat operational CONUS 4-km WRF forecasting system. Meteorol Atmos Phys 122:125–143